16th European Signal Processing Conference (EUSIPCO 2008), Lausanne, Switzerland, August 25-29, 2008, copyright by EURASIP

OVERSAMPLED DFT FILTER BANKS FOR ERROR CORRECTION CODING

Tanja Karp[1], *Michel Kieffer*[2], *and Pierre Duhamel*[2]

[1] Department of Electrical and Computer Engineering, Texas Tech University
P.O. Box 43102, Lubbock, TX, 79409, USA, tanja.karp@ttu.edu

[2] Laboratoire des Signaux et Systèmes, CNRS - SUPELEC - Univ. de Paris-Sud
91192 Gif-sur Yvette, France, kieffer@lss.supelec.fr, pierre.duhamel@lss.supelec.fr

ABSTRACT

In this paper we present a new approach to design parity-check polynomial matrices for oversampled DFT filter banks, which operate in the frequency domain and exploit the efficient polyphase structure of the filter bank. When compared to general filter banks, the design ease is significantly improved due to a reduced number of parameters, the numerical robustness of the parity check polynomial design increases, and an improved localization of errors in the observed syndroms is obtained. We apply our design to the detection of impulse errors in Gaussian background noise and evaluate the performance with respect to filter bank parameters and statistical information on the transmission channel.

1. INTRODUCTION

During the last years a growing attention was given to oversampled filter banks with perfect reconstruction (PR) [1, 2, 3, 4]. These filter banks have many advantages over critically-sampled filter banks. First, they provide increased design freedom for the synthesis filter bank: for a given analysis filter bank, the synthesis filter bank providing PR is not unique [5, 1, 6, 7]. Second, they allow higher attenuation in the stop-band [8]. Third, they may have an improved noise immunity (e.g. due to quantization of the subband signals), since the variance of the reconstruction error is inversely proportional to the oversampling factor [5, 9, 10]. Fourth, due to the redundancy between their subbands, oversampled filter banks have shown to be robust to some subbands erasures and errors. In [11] and [12], it is shown that a reconstruction of the original signal with satisfying quality is possible as long as enough subbands are present. Recently, oversampled filter banks, interpreted as error-correcting codes working in the real or complex domain, show their ability to detect and correct errors affecting the subbands samples [13, 14, 15].

When being compared to critically-sampled filter banks followed by traditional error correction codes, oversampled filter banks provide larger versatility. While in the first case the redundancy introduced by the error correction code does not improve the quality of the reconstructed signal if no errors occur during transmission, in the latter one it provides an improved quality of the reconstructed signal since aliasing is reduced in the oversampled filter bank when compared to the critically-sampled filter bank.

The main idea presented in [13] consists of building a parity-check polynomial matrix for oversampled filter banks. The part of the communication scheme between the output of the analysis filter bank and the input of the synthesis filter bank is modeled as a Gaussian-Bernoulli-Gaussian channel [16, 17]. This memoryless channel introduces a mixture of Gaussian noise of small variance (background quantization noise) and the product of a Bernoulli process with a Gaussian noise with large variance (impulse noise). Using at the receiver-side the output of the parity-check polynomial matrix, it is then possible to estimate the amplitudes and subbands affected by the realizations of the impulse noise, in spite of the presence of background noise.

Here, we concentrate on oversampled DFT filter banks [4, 7], contrary to what has been done in [13], where modulation was not considered. Modulated filter banks are interesting because of their low computational complexity when being implemented using the fast Fourier Transform (FFT). In addition, the filter bank design reduces to the design of a suitable lowpass prototype filter from which all analysis and synthesis filters are derived. We consider the same joint source-channel communication scenario and channel model as in [13]. The analysis filter bank is used at the transmitter. The encoded / quantized subband signals are then transmitted over a noisy channel. At the receiver, the synthesis filter bank reconstructs the signal and at the same time detects and corrects transmission errors with the help of parity-check polynomials. The latter need to be implemented in addition to the synthesis filter bank. In absence of quantization noise and transmission errors, i.e. when the input of the synthesis filter bank is identical to the output of the analysis filter bank, the output signals of the parity check matrices, the so called syndroms, are identical to zero. In presence of some impulse errors, the correction algorithm presented in [13] could be directly used. Nevertheless, as we show here, using the efficient polyphase structure of DFT modulated filter banks reduces the complexity of the error estimation.

The outline of the paper is as follows: In Section 2 we revisit oversampled DFT filter banks and present our new approach to calculate parity-check polynomials. Section 3 describes the considered channel model. The calculation of syndroms at the output of the parity-check polynomials is presented in Section 4. In Section 5 we derive syndrom-based detection and correction of impulse errors. The hypothesis testing applied is described in Section 6 and simulation results are shown in Section 7, before drawing some conclusions in Section 8.

2. OVERSAMPLED DFT FILTER BANKS

Figure 1 shows the efficient polyphase realization of an oversampled DFT filter bank with M subbands and a decimation factor of $N < M$ in the subbands [4]. The analysis filter bank

This work has been partly supported by the ANR DIVINE Project.

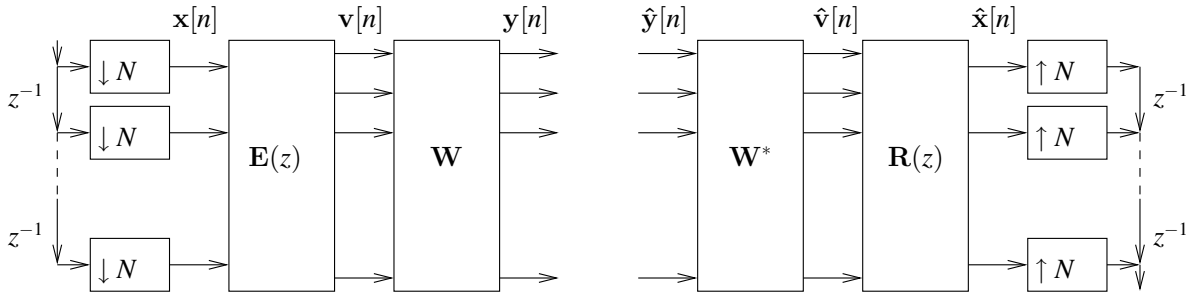

Figure 1: Polyphase realization of oversampled DFT filter bank

calculates the subband signals

$$\mathbf{Y}(z) = \mathbf{W}\mathbf{E}(z)\mathbf{X}(z) \tag{1}$$

where $\mathbf{X}(z)$ denotes the z transform of the vectorized input signal $\mathbf{x}[n] = (x[nN], x[nN-1], \ldots, x[nN-N+1])^T$, $\mathbf{Y}(z)$ the z transform of subband signals $\mathbf{y}[n] = (y_0[n], y_1[n], \ldots, y_{M-1}[n])^T$, $\mathbf{W}$ the $M \times M$ discrete Fourier transform (DFT) modulation matrix with entries $[\mathbf{W}]_{i,j} = W_M^{ij}/\sqrt{M}$ and $W_M = \exp(-j2\pi/M)$ being a complex rotation factor. $\mathbf{E}(z)$ denotes the $M \times N$ sparse polyphase filter matrix with entries

$$[\mathbf{E}(z)]_{i,j} = \begin{cases} z^{-\ell} E_{j+lN}(z^J) & \text{if } (i-\ell) \bmod b = 0 \\ 0 & \text{otherwise} \end{cases} \tag{2}$$

$$i = 0, \ldots, M-1, \quad j = 0, \ldots N-1, \quad (j+\ell N) \bmod M = i$$

with $b = \gcd(M,N)$ being the greatest common divider of M and N, $J = M/b$, and $E_k(z)$ being the kth of MN/b type-I polyphase components of the lowpass prototype filter.

At the synthesis filter bank, the signal is reconstructed from the received subband signals according to

$$\hat{\mathbf{X}}(z) = \mathbf{R}(z)\mathbf{W}^H\hat{\mathbf{Y}}(z) \tag{3}$$

where $\hat{\mathbf{Y}}(z)$ denotes the z transform of subband signals and $\mathbf{R}(z)$ of size $N \times M$ is the sparse synthesis polyphase filter matrix. For the filter bank to provide PR and be paraunitary, the following constraints apply to the polyphase matrices:

$$\mathbf{R}(z)\mathbf{E}(z) = \mathbf{I}_N, \; \mathbf{R}(z) = \tilde{\mathbf{E}}(z), \tag{4}$$

$$\tag{5}$$

with $[\tilde{\mathbf{E}}(z)]_{j,i} = [\mathbf{E}^*(1/z^*)]_{i,j}$. The PR constraints can be expressed as b independent sets for M/b subbands each [4]:

$$\tilde{\mathbf{E}}_l(z)\mathbf{E}_l(z) = \mathbf{I}_{N/b}, \quad l = 0, \ldots, b-1 \tag{6}$$

where $\mathbf{E}_l(z)$ is of size $J \times N/b$ and has the following entries:

$$[\mathbf{E}_l(z)]_{i,j} = [\mathbf{E}(z)]_{l+ib,l+jb} \tag{7}$$

In the following we restrict ourselves to paraunitary oversampled DFT filter banks with a linear phase FIR (finite impulse response) prototype filter of length L.

2.1 Calculation of Parity Check Polynomials

The mathematical framework to derive parity check polynomials from the filter bank polyphase matrix was already presented in [13]. The general scheme is shown in Figure 2, where $\hat{\mathbf{y}}[n]$ denotes the vector of subband signals and $\mathbf{s}[n]$ the vector of the $M-N$ syndroms created. However, in this approach the polyphase decomposition of a general oversampled filter bank was considered and for non-integer factors of oversampling the parity-check polynomials have to be calculated through QR factorization. The major drawback of the approach is the relatively high order of the resulting parity check polynomials and thus a bad time localization of impulse errors.

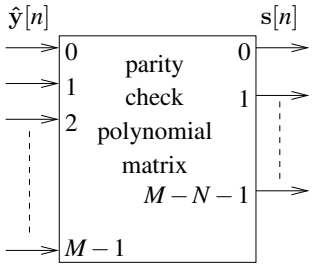

Figure 2: Parity check polynomials at synthesis filter bank as proposed in [13]

We here exploit the efficient realization of oversampled DFT filter banks with a sparse polyphase filter matrix as shown in Figure 1. Instead of calculating the syndroms directly from the subband signals, we first perform the inverse DFT at the synthesis filter bank and then calculate the syndroms in the frequency domain from $\hat{\mathbf{v}}[n]$. The design of the $M-N$ parity check polynomials can now be split into the independent calculation of b parity-check polynomial matrices $\tilde{\mathbf{C}}_l(z)$ of size $(M-N)/b \times J$, which are obtained by expanding $\mathbf{E}_l(z)$ from (7) to a $J \times J$ square paraunitary matrix

$$\begin{bmatrix} \tilde{\mathbf{E}}_l(z) \\ \tilde{\mathbf{C}}_l(z) \end{bmatrix} [\mathbf{E}_l(z) \quad \mathbf{C}_l(z)] = \mathbf{I}_J \tag{8}$$

A prototype filter design algorithm which automatically calculates $\mathbf{C}_l(z)$ can be found in [4]. Alternatively, for a given prototype filter, $\mathbf{C}_l(z)$ can be calculated through QR factorization of $\mathbf{E}_l(z)$, similarly to [13] but using matrices of significantly smaller size. Note that since $\mathbf{E}_l(z)$ contains

shifted polynomials in z^J, see (7), so does $\mathbf{C}_l(z)$, i.e. most of its entries are zeros. Thus, for a prototype filter of length L the b parity-check polynomial matrices $\tilde{\mathbf{C}}_l(z)$ contain a total of $\lceil L(M-N)/N \rceil$ non-zero entries. Note that with the approach from [13] we would obtain a parity-check polynomial matrix of size $M \times (M-N)$ and order L/N. Using the new approach, the number of multiplications performed to calculate the syndroms is thus reduced by a factor of M.

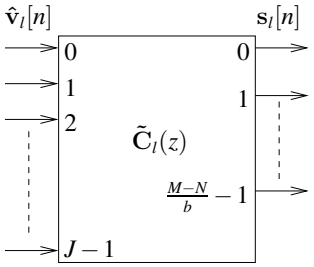

Figure 3: New parity check polynomials

3. CHANNEL MODEL

In communication contexts, the samples at the output of the analysis filter bank encounter several processing steps before being transmitted over the channel (quantization, entropy coding, channel coding, modulation...). Here, as in [17], the part of the communication scheme between the output of the analysis filter bank and the input of the synthesis filter bank is represented by a Gaussian-Bernoulli-Gaussian channel [16]. More precisely, we assume that $\hat{\mathbf{y}}[n]$ is corrupted by two independent noise sources:

1. Gaussian background noise caused by quantization. It is modeled as i.i.d. Gaussian noise with zero mean and identical variance σ_g^2 in all subbands.
2. Bernoulli-Gaussian impulse noise due to non-corrected channel noise and amplified by inverse quantization. Impulses occur with probability p_i and are assumed equally likely in all subbands. Thus, in each subband a Gaussian noise with zero mean and variance σ_i^2 is multiplied with a Bernoulli sequence of i.i.d. zeros and ones, where the probability of a one is p_i.

More details about this channel model and its validity for various actual communication channels can be found in [13, 17].

4. SYNDROM CALCULATION AND PROPERTIES

The outputs of the parity check polynomials are called the syndroms. In the case where $\hat{\mathbf{y}}[n] = \mathbf{y}[n]$, i.e. where no quantization of the subband signals is performed and no impulse errors occur, all syndroms are equal to zero. In the presence of both noise sources, the syndroms $s_{l,j}[n]$ are composed of a term $s^g_{l,j}[n]$ due to the Gaussian background noise and a term $s^i_{l,j}[n]$ caused by the impulse noise.

$$s_{l,j}[n] = s^g_{l,j}[n] + s^i_{l,j}[n], \tag{9}$$
$$l = 0,\dots,b-1, \quad j = 0,\dots,\frac{M-N}{b}-1$$

4.1 Syndroms Generated by Gaussian Noise

For the part $s^g_{l,j}[n]$ of the syndroms caused by the Gaussian background noise modelling the quantization error, it can be easily shown that they have an i.i.d. Gaussian distribution with the same variance σ_g^2 as the Gaussian background noise.

4.2 Syndroms Generated by Impulse Noise

Let's consider that a single, complex valued noise impulse a is present in subband η at time instance κ. After performing the inverse DFT, the impulse error is spread over all subbands and is then fed into the parity check polynomials in order to calculate the syndroms. This is the main difference with [13], where the impulse error enters directly the parity-check polynomial matrix.

The syndroms caused from this error are given by

$$s^i_{l,i}[n] = \frac{a}{\sqrt{M}} \sum_{j=0}^{J-1} \tilde{c}_{l,(i,j)}[n-\kappa] W_M^{-(l+jb)\eta} \tag{10}$$
$$l = 0,\dots b-1, \quad i = 0,\dots \frac{M-N}{b}-1$$

Thus, a single impulse error is affecting the syndrom at $L_{l,i}$ taps, where $L_{l,i}$ is determined by the number of values n for which

$$\sum_{j=0}^{J-1} \tilde{c}_{l,(i,j)}[n-\kappa] W_M^{-(l+jg)\eta} \neq 0 \tag{11}$$

We gather all these values in a syndrom vector $\mathbf{s}^i_{l,i}[\kappa]$ with

$$\mathbf{s}^i_{l,i}[\kappa] = \begin{bmatrix} s^i_{l,i}[\kappa - \kappa_{L_{l,i}-1}] \\ s^i_{l,i}[\kappa - \kappa_{L_{l,i}-2}] \\ \vdots \\ s^i_{l,i}[\kappa - \kappa_{l,i,0}] \end{bmatrix} = a \cdot \mathbf{q}_{l,i}[\eta] \tag{12}$$
$$l = 0,\dots b-1, \quad i = 0,\dots \frac{M-N}{b}-1$$

with

$$\mathbf{q}_{l,i}[\eta] = \frac{1}{\sqrt{M}} \sum_{j=0}^{J-1} W_M^{-(l+jg)\eta} \begin{bmatrix} \tilde{c}_{l,(i,j)}[-\kappa_{L_{l,i}+1}] \\ \tilde{c}_{l,(i,j)}[-\kappa_{L_{l,i}+2}] \\ \vdots \\ \tilde{c}_{l,(i,j)}[-\kappa_{l,i,0}] \end{bmatrix} \tag{13}$$

Note that $\mathbf{q}_{l,i}[\eta]$ is a signature waveform that only depends on the filter bank parameters (and thus parity check polynomials), the subband index η in which the error occurred, and the indices l, and i. It can be pre-calculated and stored for each value of η.

Concatenation of all $(M-N)$ syndroms to one results in one syndrom vector $\mathbf{s}^i[\kappa] = a \cdot \mathbf{q}[\eta]$. It can be easily shown that $||\mathbf{q}_{l,i}[\eta]||^2 = ||\tilde{\mathbf{c}}_{l,i}[n]||^2/M = 1/M$ and thus $||\mathbf{q}[n]||^2 = (M-N)/M$. We denote the length of $\mathbf{q}[\eta]$ as L_c.

5. IMPULSE ERROR DETECTION

In the following we assume that the impulse error occurrence rate is low enough that we can discard the case that a syndrom vector $\mathbf{s}[\kappa]$ is corrupted by more than one impulse. If a

complex impulse a is present at time instant κ in subband η we observe:

$$\mathbf{s}[\kappa] = \mathbf{s}^g[\kappa] + \mathbf{s}^i[\kappa] = \mathbf{s}^g[\kappa] + a\mathbf{q}[\eta] \tag{14}$$

To estimate the subband in which the impulse error occurred and its value, we maximize the *a posteriori* probability density function $f(a,\eta|\mathbf{s}[\kappa])$.

$$f(a,\eta|\mathbf{s}[\kappa]) = \frac{f(\mathbf{s}[\kappa]|a,\eta)f(a,\eta)}{f(\mathbf{s}[\kappa])} \tag{15}$$

with

$$f(a,\eta) = f(a)f(\eta) = \frac{1}{M\sqrt{2\pi\sigma_i^2}}\exp\left(-\frac{|a|^2}{2\sigma_i^2}\right) \tag{16}$$

In the above equation $f(\mathbf{s}[\kappa])$ is simply a normalizing constant and can be discarded in the estimation. If a single impulse error of amplitude a is present in subband η at time κ, then after subtracting the error waveform caused by the impulse error from the syndrom, the remaining syndrom is caused by the Gaussian background noise.

$$f(\mathbf{s}^g[\kappa]|a,\eta) = f(\mathbf{s}[\kappa] - a\mathbf{q}[\eta]|a,\eta) \tag{17}$$

$$= \frac{1}{(2\pi\sigma_g^2)^{L_c/2}}\exp\left(-\frac{||\mathbf{s}^g[\kappa])||^2}{2\sigma_g^2}\right) \tag{18}$$

$$= \frac{1}{(2\pi\sigma_g^2)^{L_c/2}}\exp\left(-\frac{(\mathbf{s}[\kappa] - a\mathbf{q}[\eta])^H(\mathbf{s}[\kappa] - a\mathbf{q}[\eta])}{2\sigma_g^2}\right) \tag{19}$$

Thus, we calculate

$$(\hat{a},\hat{\eta}) = \arg\max_{(a,\eta)} f(\mathbf{s}[\kappa] - a\mathbf{q}[\eta]|a,\eta)f(a,\eta) \tag{20}$$

$$= \arg\max_{(a,\eta)} \exp\left(-\frac{(\mathbf{s}[\kappa] - a\mathbf{q}[\eta])^{\mathrm{H}}(\mathbf{s}[\kappa] - a\mathbf{q}[\eta])}{2\sigma_g^2} - \frac{|a|^2}{2\sigma_i^2}\right) \tag{21}$$

$$= \arg\max_{(a,\eta)} (g(a,\eta)) \tag{22}$$

with

$$g(a,\eta) = -\frac{(\mathbf{s}[\kappa] - a\mathbf{q}[\eta])^{\mathrm{H}}(\mathbf{s}[\kappa] - a\mathbf{q}[\eta])}{2\sigma_g^2} - \frac{|a|^2}{2\sigma_i^2}$$

$$= -\frac{||\mathbf{s}[\kappa]||^2 + |a|^2\frac{M-N}{M} - a^H\mathbf{q}^H[\eta]\mathbf{s}[\kappa] - a\mathbf{s}[\kappa]^H\mathbf{q}[\eta]}{2\sigma_g^2} - \frac{|a|^2}{2\sigma_i^2}$$

For all possible subbands $\eta = 0,\ldots,M-1$ in which the error could occur, we calculate $\hat{a}(\eta)$ from

$$\frac{\partial}{\partial a^H}(g(a,\eta)) = 0 \quad \Rightarrow \quad \hat{a}(\eta) = \frac{\mathbf{q}^H[\eta]\mathbf{s}[\kappa]}{\frac{M-N}{M} + \frac{\sigma_g^2}{\sigma_i^2}} \tag{23}$$

To find the optimal subband $\hat{\eta}$, we plug (23) back into (21) and obtain $\hat{\eta}$ as:

$$\hat{\eta} = \arg\max_{(\hat{a}(\eta))}\left(\frac{-||\mathbf{s}[\kappa]||^2 + |\hat{a}(\eta)|^2\left(\frac{M-N}{M} + \frac{\sigma_g^2}{\sigma_i^2}\right)}{2\sigma_g^2}\right) \tag{24}$$

Thus, out of all M possible subband choices, the subband $\hat{\eta}$ is chosen for which $|\hat{a}(\eta)|$ is the largest.

6. HYPOTHESIS TESTING

To determine if an impulse error is present, the following hypothesis test is performed: We observe the syndrom vector $\mathbf{s}[n]$ over a sliding window of size L_c and calculate $\hat{a}(\hat{\eta})$ according to (23) and (24). We decide that an error of amplitude $\hat{a}$ is present in subband $\hat{\eta}$ and time instant κ if

$$\Lambda(\mathbf{s}[\kappa]) = \ln\left(\frac{f(\mathbf{s}[\kappa]|\hat{a}(\hat{\eta}))}{f(\mathbf{s}[\kappa]|\text{no error})}\right) \tag{25}$$

$$= \frac{|\hat{a}|^2}{2\sigma_g^2}\left(\frac{M-N}{M} + 2\frac{\sigma_c^2}{\sigma_b^2}\right) > \alpha \tag{26}$$

Note that this test disregards the possibility that more than one impulse error affected the syndrom within the observed window. Thus the probability p_i of an impulse error has to be sufficiently low.

7. SIMULATION RESULTS

We simulated receiver operating curves (ROC) for the following case: The PR DFT filter bank has $M = 8$ subbands and a decimation factor of $N = 6$. Two different linear-phase prototype filters are considered, one with a length of $L = 24$ samples and one with a length of $L = 48$ samples. The two prototype filters are shown in Figure 4.

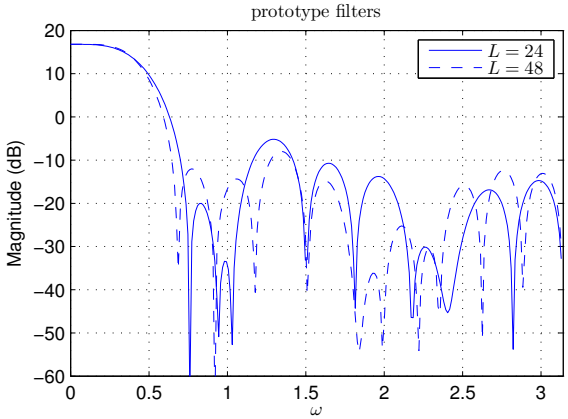

Figure 4: Prototype filter frequency responses

The parity check polynomials $\tilde{\mathbf{C}}_l(z)$ contain shifted polynomials in z^4 and have 1 (2) non-zero coefficients per polynomial for $L = 24$ ($L = 48$). An impulse error thus creates a signature waveform of length $L_c = 8$ (16). This is $J = 4$ times shorter than using the approach from [13].

We use a complex input signal with zero mean and variance $\sigma_x^2 = 1$. The vector $\hat{\mathbf{y}}[n]$ was obtained from $\mathbf{y}[n]$ by adding complex noise according to the described channel model. For all simulations we kept the variance of the impulse noise at $\sigma_i^2 = 1$ and its probability of occurrence at $p_i = 0.001$. We varied the variance of the complex quantization noise from $\sigma_g^2 = 0.001$ to $\sigma_g^2 = 0.1$. Figure 5 shows the resulting experimental ROC's, where P_F and P_D denote the false alarm and detection probability, respectively.

It can be seen that there is hardly any difference in performance between the two prototype filters of different lengths. Also, the larger the ratio σ_i^2/σ_g^2 the better is the performance in terms of error detection. False alarms occur when the quantization noise in absence of an impulse error causes

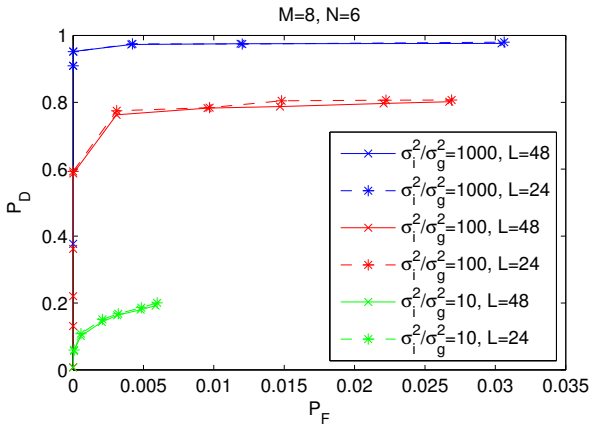

Figure 5: Experimental ROC curves for $M = 8$ and $N = 6$

(26) to pass the threshold α. The reduction in the detection rate with decreasing ratio σ_i^2/σ_g^2 has two reasons: first, it is more difficult to distinguish impulse errors from quantization noise, i.e., the percentage of impulse errors with an amplitude that is significantly higher than that of the background noise reduces. Low amplitude impulse errors are not detected, but need not to be corrected either, since they are harmless for the reconstructed signal. Second, in presence of an impulse error, the probability of determining an incorrect subband $\hat{\eta}$ in (24) increases.

Table 1 shows experimental results for the SNR in dB obtained at the synthesis filter bank output using the prototype filter of length $L = 24$. For $\alpha = \infty$ no impulse errors are corrected. SNR_g describes the SNR obtained in absence of impulse errors, i.e. the best achievable case if all impulse errors are corrected. For large α the error correction works nearly perfectly. However, as α decreases, the increased false alarm rate reduces the performance to a point where it is worse than without impulse error correction.

ideal case	error correction with $\alpha\sigma_g^2$					
	∞	100	50	20	15	10
$\text{SNR}_g = 30$	27	29.9	29.9	29.5	29.0	28.3
$\text{SNR}_g = 20$	19.6	19.9	19.9	19.7	19.2	18.5

Table 1: SNR in dB with impulse correction for $p_i = 0.001$.

8. CONCLUSIONS

In this paper we have presented a new approach to calculate parity check polynomial matrices for oversampled DFT filter banks. We have then applied it to the correction of impulse channel errors and have shown simulation results. The analytical calculation of ROC curves and the extension of the presented framework to cases with a higher rate of impulse errors is the focus of future research.

REFERENCES

[1] Z. Cvetkovic and M. Vetterli. Oversampled filter banks. *IEEE Trans. on Signal Processing*, 46(5):1245–1255, 1998.

[2] J. Kliewer and A. Mertins. Oversampled cosine-modulated filter banks with arbitrary system delay. *IEEE Trans. on Signal Processing*, 46(4):941–955, 1998.

[3] H. Bölcskei and F. Hlawatsch. Oversampled cosine modulated filter banks with perfect reconstruction. *IEEE Trans. on Circuits and Systems II*, 45(8):1057–1071, 1998.

[4] K. Eneman and M. Moonen. DFT modulated filter bank design for oversampled subband systems. *Signal Processing*, 81:1947–1973, 2001.

[5] H. Bölcskei, F. Hlawatsch, and H. G. Feichtinger. Frame-theoretic analysis of oversampled filter banks. *IEEE Trans. on Signal Processing*, 46(12):3256–3268, 1998.

[6] F. Labeau. *Errors and Losses in Image Transmission: Error-Correcting and Recovering Schemes*. PhD thesis, Université Catholique de Louvain, Louvain-la-Neuve, 2000.

[7] S. Weiss, S. Redif, T. Cooper, C. Liu, P. D. Baxter, and J. G. McWhirter. Paraunitary oversampled filter bank design for channel coding. *EURASIP Journal on Applied Signal Processing*, 2006(Article ID 31346):1–10, 2006.

[8] Toshihisha Tanaka and Yukihiko Yamashita. The generalized lapped pseudo-biorthogonal transform. In *ICASSP*, vol. II, pp. 1273–1276, Orlando, FL, 2002.

[9] V. K. Goyal and J. Kovacević. Generalized multiple description coding with correlating transforms. *IEEE Trans. on Information Theory*, 47(6):2199–2224, 2001.

[10] H. Bölcskei and F. Hlawatsch. Noise reduction in oversampled filter banks using predictive quantization. *IEEE Trans. on Information Theory*, 47(1):155–172, 2001.

[11] V. K Goyal, J. Kovacević, and J. A. Kelner. Quantized frame expansions with erasures. *Journal of Appl. and Comput. Harmonic Analysis*, 10(3):203–233, 2001.

[12] J. Kovacević, P. L. Dragotti, and V. K Goyal. Filter bank frame expansions with erasures. *IEEE Trans. on Information Theory*, 48(6):1439–1450, 2002.

[13] F. Labeau, J.-C. Chiang, M. Kieffer, P. Duhamel, L. Vandendorpe, and B. Macq. Oversampled filter banks as error correction codes: Theory and impulse noise correction. *IEEE Trans. on Signal Processing*, 53(12):4619 – 4630, 2005.

[14] S. Marinkovic and C. Guillemot. Joint source-channel coding based on cosine-modulated filter banks for erasure-resilient signal transmission. *EURASIP Journal on Applied Signal Processing*, 2005(Article ID 82023):510–524, 2005.

[15] S. Marinkovic and C. Guillemot. Joint source-channel coding by means of an oversampled filter bank code. *EURASIP Journal on Applied Signal Processing*, 2006(Article ID 82023):1–12, 2006.

[16] M. Ghosh. Analysis of the effect of impulsive noise on multicarrier and single carrier QAM systems. *IEEE Trans. on Communications*, 44(2):145–147, 1996.

[17] A. Gabay, M. Kieffer, and P. Duhamel. Joint source-channel coding using real BCH codes for robust image transmission. *IEEE Trans. on Image Processing*, 16(6):1568–1583, 2007.